Journal of Power Sources 245 (2014) 816–821

Contents lists available at SciVerse ScienceDirect

Journal of Power Sources

journal homepage: www.elsevier.com/locate/jpowsour

High potential durability of $LiNi_{0.5}Mn_{1.5}O_4$ electrodes studied by surface sensitive X-ray absorption spectroscopy

Hiroyuki Kawaura [a,*], Daiko Takamatsu [a], Shinichiro Mori [b], Yuki Orikasa [b], Hidetaka Sugaya [a], Haruno Murayama [a], Kouji Nakanishi [a], Hajime Tanida [a], Yukinori Koyama [a], Hajime Arai [a], Yoshiharu Uchimoto [b], Zempachi Ogumi [a]

[a] Office of Society-Academia Collaboration for Innovation, Kyoto University, Gokasho, Uji, Kyoto 611-0011, Japan
[b] Graduate School of Human and Environmental Studies, Kyoto University, Yoshida-Nihonmatsu, Sakyo, Kyoto 606-8501, Japan

HIGHLIGHTS

- Phenomena at electrode/electrolyte interface were studied by *in situ* TRF-XAS.
- Polycrystalline thin films of $LiNi_{0.5}Mn_{1.5}O_4$ were deposited by PLD technique.
- Surface of $LiNi_{0.5}Mn_{1.5}O_4$ is stable against reduction by electrolyte solutions.
- Decomposition of electrolyte solutions is observed by XPS.
- $LiNi_{0.5}Mn_{1.5}O_4$ has good cycling characteristics during high operating potential.

ARTICLE INFO

Article history:
Received 12 April 2013
Received in revised form
6 June 2013
Accepted 3 July 2013
Available online 10 July 2013

Keywords:
$LiNi_{0.5}Mn_{1.5}O_4$
In situ XAS
Thin film electrode
Protective surface layer
Lithium–ion battery

ABSTRACT

Phenomena at electrode/electrolyte interface of $LiNi_{0.5}Mn_{1.5}O_4$ are studied by *in situ* total-reflection fluorescence X-ray absorption spectroscopy (TRF-XAS), *ex situ* X-ray photoelectron spectroscopy (XPS), and electrochemical tests. Flat and well-defined thin films of $LiNi_{0.5}Mn_{1.5}O_4$ prepared by pulsed laser deposition (PLD) are used as model electrodes to facilitate the observation of the interface. The thin-film $LiNi_{0.5}Mn_{1.5}O_4$ electrode showed good cycling characteristics at around 4.7 V vs. Li/Li^+. The TRF-XAS measurements reveal that nickel and manganese species at the surface have almost the same chemical states and local environments as those in the bulk when in contact with organic electrolyte solutions (1 mol dm^{-3} $LiClO_4$ in a 1:1 volumetric mixture of ethylene carbonate and diethyl carbonate). This is in sharp contrast to the behavior of a $LiCoO_2$ electrode, in which the surface cobalt species is irreversibly reduced by soaking to the organic electrolyte solutions, leading to gradual material deterioration during the delithiation/lithiation cycling (D. Takamatsu et al., Angew. Chem. Int. Edit., 51 (2012) 11597). It is suggested that the electrolyte decomposition products detected by XPS form a protective layer to restrict the reduction of the surface species of $LiNi_{0.5}Mn_{1.5}O_4$, leading to good cycling characteristics of $LiNi_{0.5}Mn_{1.5}O_4$ in spite of its high operating potential.

1. Introduction

The development of rechargeable lithium–ion batteries (LIBs) that provide high power density and durability is important to meet demands for high-power applications such as electric vehicles, hybrid vehicles and aerospace applications, and high-performance positive electrode materials for such advanced LIBs are indispensable. For possible positive electrode materials, transition metal substituted spinel materials $LiM_xMn_{2-x}O_4$ (M = Cr, Fe, Co, Ni, Cu, etc.) have gained much attention because of their high working potential of around 5 V versus Li/Li^+ [1–9]. Among them, $LiNi_{0.5}Mn_{1.5}O_4$ is of special interest thanks to its high discharge capacity of ca. 120 mAh g^{-1} with the average potential of ca. 4.7 V [7–9].

$LiNi_{0.5}Mn_{1.5}O_4$ electrodes generally show comparatively good cycling characteristics [2,7–9], although it is anticipated that oxidative electrolyte decomposition could occur under such high operating potential. The reason for the acceptable durability could be related to surface film formation, as has been suggested by *ex situ* analytical methods such as transmission electron microscopy

* Corresponding author. Tel.: +81 774 38 4969; fax: +81 774 38 4996.
E-mail address: kawaura@rising.saci.kyoto-u.ac.jp (H. Kawaura).

0378-7753/$ – see front matter © 2013 Elsevier B.V. All rights reserved.
http://dx.doi.org/10.1016/j.jpowsour.2013.07.011

(TEM), Fourier transform infrared spectroscopy (FT-IR), Raman spectroscopy, and X-ray photoelectron spectroscopy (XPS) [9–14]. However the detailed mechanism of the durability is unclear yet. The cycling characteristics of LIBs are generally affected by the nature and phenomena at the interface between the electrode and electrolyte, especially in the positive electrode side [10]. Suitable *in situ* analysis techniques to observe the interface phenomena under battery operating conditions are desirable but have not been well established. A high space resolution is required to focus the nano-scale interface domain between the huge bulk of the electrode and the electrolyte.

Recently, our group has applied a surface sensitive *in situ* analytical method, total-reflection fluorescence X-ray absorption spectroscopy (TRF-XAS), to observe electrode/electrolyte interface under battery operating conditions [15]. This method utilizes flat and well-defined thin films as model electrodes to facilitate the observation of the electrode surface, instead of composite electrodes (consisting of active materials, electric conductive materials and binders) that have rough and poorly defined surfaces. The fluorescence signals under total reflection conditions effectively offer information at the interfaces of the electrodes. Our group has shown using this technique that the surface cobalt species of $LiCoO_2$ electrodes is reduced when the electrodes are in contact with organic electrolyte solutions, and that this can be the initial deterioration process of LIBs during the course of charge/discharge cycling [15]. Because such reductive behavior at the surface is observed for the 4 V class positive electrode material of $LiCoO_2$, it is interesting to detail the surface behavior of the $LiNi_{0.5}Mn_{1.5}O_4$ electrodes that show much higher potential. By conducting *in situ* observation of the interfacial phenomena, it is expected to obtain the information on the durability of this high potential material.

In this report we studied the phenomena at the $Li_{1-x}Ni_{0.5}Mn_{1.5}O_4$ electrode/electrolyte interface using $LiNi_{0.5}Mn_{1.5}O_4$ thin films as model electrodes. The polycrystalline thin films were deposited on platinum substrates by pulsed laser deposition (PLD) technique. The outermost surface and bulk behavior of the electrodes was observed using the TRF-XAS method both before and after electrolyte soaking and during the charging process to 4.9 V. The durability of the $LiNi_{0.5}Mn_{1.5}O_4$ electrodes is discussed using the results from TRF-XAS, electrochemical tests and *ex situ* XPS for the surface film analysis.

2. Experimental

$LiNi_{0.5}Mn_{1.5}O_4$ thin films were deposited on flat platinum substrates by the PLD method. The platinum substrates were mechanically polished polycrystals. The target used for the PLD was rich in lithium by 50 mol% to the stoichiometric composition to compensate the loss of lithium during the deposition. The substrates were heated at 873 K during the deposition and oxygen partial pressure was fixed at 26.6 Pa. Laser ablation was performed using a Nd:YAG laser with a wavelength of 266 nm at a power of 200 mW, and pulse irradiation frequency was fixed at 10 Hz. The composition of the thin films was analyzed to be Li:Ni:Mn = 34.1:15.8:50.1 in mol by inductively coupled plasma (ICP) spectrometry, while the chemical formula of the thin films is simply described as $LiNi_{0.5}Mn_{1.5}O_4$ hereafter.

Structure of the $LiNi_{0.5}Mn_{1.5}O_4$ thin films was characterized by X-ray diffraction (XRD), Raman spectroscopy, and TEM. The XRD patterns were recorded using a Cu Kα radiation (Rigaku SmartLab) in the range of $2\theta = 10–70^\circ$. The Raman spectra were recorded using a focused 514 nm laser beam (Horiba Jobin-Yvon, LabRam HR-800). The cross sections of the $LiNi_{0.5}Mn_{1.5}O_4$ thin films were observed by TEM (JEOL, JEM 2100F) with tungsten coating as protective films.

Electrochemical measurements were conducted by cyclic voltammetry (CV) in the potential range of 4.4–4.9 V versus Li/Li^+ with a scan rate of 0.2 mV s^{-1}. Three-electrode electrochemical cells were composed of a $LiNi_{0.5}Mn_{1.5}O_4$ thin film as a working electrode with an active area of ca. 0.50 cm^2, lithium foil as counter and reference electrodes, and 1 mol dm^{-3} solution of $LiClO_4$ dissolved in a 1:1 volumetric mixture of ethylene carbonate (EC) and diethyl carbonate (DEC) as an electrolyte.

The surface of the $LiNi_{0.5}Mn_{1.5}O_4$ thin films was analyzed before and after charge/discharge cycling by XPS using an Al Kα radiation (ULVAC-PHI, Quantera SXM). The XPS apparatus was connected to an argon-filled glove-box through a transfer chamber so that the thin-film electrodes were placed on sample holders without exposure to moisture or air after disassembled from the electrochemical cells. The measured spectra were analyzed by Multipak software. The peak in the C-1s region corresponding to universal carbon contamination was set at 284.8 eV to calibrate binding energy.

In situ TRF-XAS was conducted at Ni and Mn K-edges using the beamlines BL01B1 and BL28XU, SPring-8 (Hyogo, Japan). Spectro-electrochemical cells [15] were composed of a $LiNi_{0.5}Mn_{1.5}O_4$ thin film as a working electrode, lithium foil as a counter electrode, 1 mol dm^{-3} $LiClO_4$ dissolved in a 1:1 volumetric mixture of EC and DEC as an electrolyte, and a microporous polypropylene membrane (Celgard 3501) as a separator. The cells were completely sealed, and the free space in the cells was filled with helium. Electrochemical lithium deintercalation was performed by linear sweep voltammetry with a scan rate of 0.2 mV s^{-1}. The fluorescence signals were collected by a 19-element solid-state detector. Calculated critical angle of the total reflection for the Ni K-edge of $LiNi_{0.5}Mn_{1.5}O_4$ was 0.28°. The calculation method was described in Supporting Information of Ref. [15]. Ni K-edge fluorescence XAS spectra were measured at an incident angle of 0.2° for the surface of the $LiNi_{0.5}Mn_{1.5}O_4$ thin films, and penetration depth was estimated to be ca. 3 nm in this condition. As the critical angle of the total reflection for the Mn K-edge is higher than that for the Ni K-edge, the same incident angle of 0.2° was used for the Mn K-edge fluorescence XAS for the surface. To measure XAS spectra for the bulk of the $LiNi_{0.5}Mn_{1.5}O_4$ thin films at both Ni and Mn K-edges, an incident angle of 2.0° was used, and the penetration depth was estimated to be greater than 100 nm. Intensity of the XAS spectra was normalized at the points 200 eV above from the absorption edge.

3. Results and discussion

3.1. Structure characterization

An XRD pattern of the $LiNi_{0.5}Mn_{1.5}O_4$ thin film on the platinum substrate is shown in Fig. 1. All the observed peaks can be indexed to either the diffraction from a spinel structure ($a = 8.186$ Å) or that from the platinum substrate. No impurity phase is observed. The diffraction peaks from the spinel phase are very sharp, indicating that the $LiNi_{0.5}Mn_{1.5}O_4$ thin films have a high degree of crystallinity. It has been reported that $LiNi_{0.5}Mn_{1.5}O_4$ has two kinds of crystallographic symmetries; *Fd*-3*m* space group of a conventional spinel structure with disordered Ni/Mn arrangement and $P4_332$ space group of an ordered spinel [16–19]. Raman spectroscopy was carried out to examine the crystallographic symmetry of the $LiNi_{0.5}Mn_{1.5}O_4$ thin films. It is reported that the $P4_332$ structure exhibits a clear triplet of peaks in the range of 550–700 cm^{-1} in Raman spectra, while the *Fd*-3*m* structure exhibits a pair of broad and sharp peaks there [16,20]. In addition, only the $P4_332$ structure exhibits a pair of peaks at 200–250 cm^{-1}. Raman spectra of the $LiNi_{0.5}Mn_{1.5}O_4$ thin films exhibit sharp peaks at 497 and 636 cm^{-1}

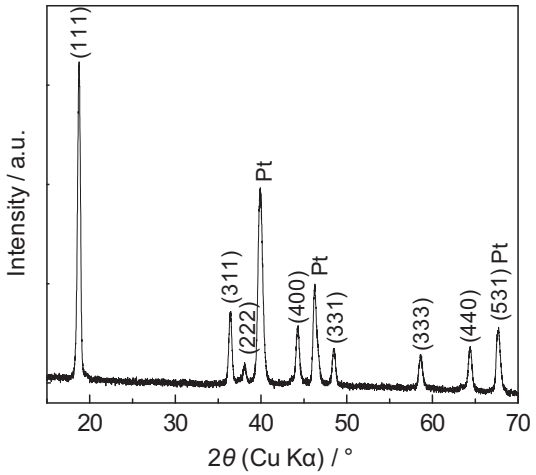

Fig. 1. XRD pattern of the $LiNi_{0.5}Mn_{1.5}O_4$ thin film on the platinum substrate with the diffraction indices from a spinel structure.

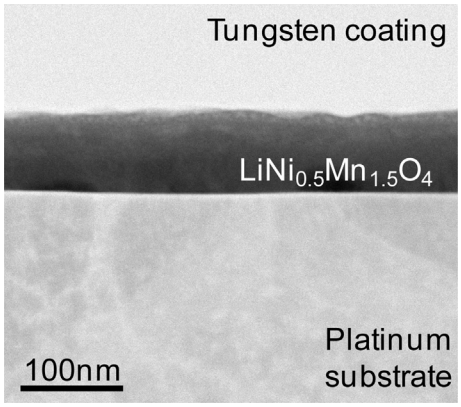

Fig. 3. Cross-sectional TEM image of the $LiNi_{0.5}Mn_{1.5}O_4$ thin film.

and broad ones at 335, 396 and 605 cm^{-1} as shown in Fig. 2. The broad peak at 605 cm^{-1} and no peaks at 200–250 cm^{-1} clearly indicate that the $LiNi_{0.5}Mn_{1.5}O_4$ thin films of this study have the disordered spinel structure with the *Fd*-3*m* space group. The XRD pattern shown in Fig. 1 exhibits no peaks of (110), (320), (510) or (522) diffraction, which are additionally observed for the $P4_332$ structure [18,19]. This is also consistent with that the $LiNi_{0.5}Mn_{1.5}O_4$ thin films have the disordered spinel structure. Fig. 3 shows a cross-sectional TEM image of the $LiNi_{0.5}Mn_{1.5}O_4$ thin film on the platinum substrate with tungsten coating. The thin films are well dense and flat, and no notable defect is observed. The film thickness is estimated to be ca. 70 nm from the TEM observation.

3.2. Electrochemical behavior

Electrochemical behavior of the $LiNi_{0.5}Mn_{1.5}O_4$ thin-film electrodes was examined by CV measurements. Fig. 4 shows typical CV curves of the 1st, 10th and 50th cycles for the $LiNi_{0.5}Mn_{1.5}O_4$ thin-film electrodes cycled between 4.4 and 4.9 V versus Li/Li^+. During the first charging, a small peak of the current is observed at 4.03 V (not shown), suggesting that the $LiNi_{0.5}Mn_{1.5}O_4$ thin films contain a small amount of Mn^{3+} species and oxygen deficiency. Well-resolved reversible peaks of the current are observed at 4.70 and 4.78 V in the charging process and at 4.65 and 4.69 V in the discharging one. The double peaks at ca. 4.7 V correspond to the two-step redox reactions for $LiNi_{0.5}Mn_{1.5}O_4/Li_{0.5}Ni_{0.5}Mn_{1.5}O_4$ and $Li_{0.5}Ni_{0.5}Mn_{1.5}O_4/Ni_{0.5}Mn_{1.5}O_4$ [21]. The peak current for the $LiNi_{0.5}Mn_{1.5}O_4$ thin-film electrodes is kept at ca. 85% of the 1st cycle at the 50th cycle, and no notable increase in polarization is observed.

Good cycling characteristics of the $LiNi_{0.5}Mn_{1.5}O_4$ thin-film electrodes can also be seen in capacity retention in cycles. Fig. 5 shows the charge/discharge capacity and corresponding coulombic efficiency in the CV cycles for the $LiNi_{0.5}Mn_{1.5}O_4$ thin-film electrodes. In the initial few cycles, notable irreversible capacity was observed. After that, the coulombic efficiency was still somewhat low, e.g. 90% in the 10th cycle, but the retention of the discharge capacity is high, e.g. 85% in the 50th cycle as compared with the 1st cycle. The low coulombic efficiency suggests side reactions, possibly oxidative decomposition of the organic electrolyte solutions, in the CV cycles. The coulombic efficiency gradually increased by the CV cycles, which can be ascribed to that the side reactions caused the formation of a protective surface layer on the thin-film electrodes. In spite of the low coulombic efficiency, the good cycling characteristic in terms of the retention of the discharge capacity is significant, since thin-film electrodes are expected to show accelerated deterioration of electrochemical performance due to significantly larger surface to volume ratio of electrode/electrolyte interface than conventional composite electrodes consisting of powder active materials; the authors have reported insufficient cycle durability of the

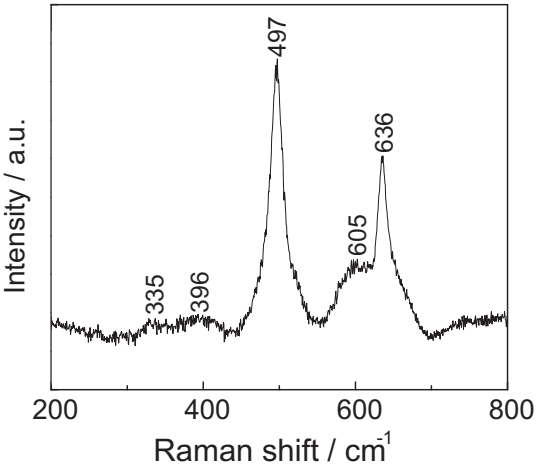

Fig. 2. Raman spectrum of the $LiNi_{0.5}Mn_{1.5}O_4$ thin film.

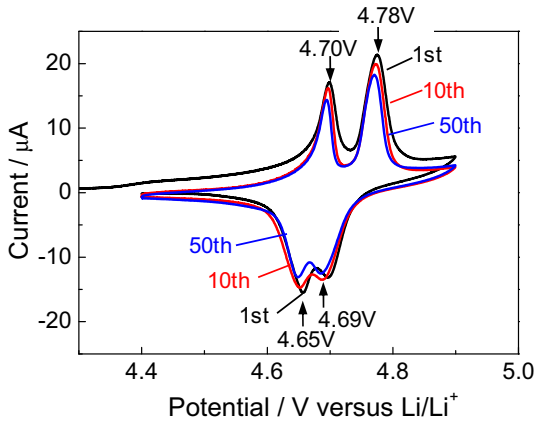

Fig. 4. Cyclic voltammograms of the 1st, 10th and 50th cycles for the $LiNi_{0.5}Mn_{1.5}O_4$ thin-film electrode on the platinum substrate in a potential range of 4.4–4.9 V versus Li/Li^+ with a scan rate of 0.2 mV s^{-1}.

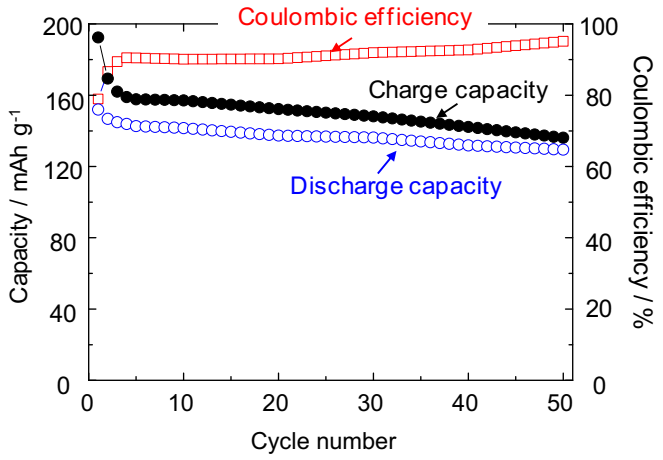

Fig. 5. Charge/discharge capacity and coulombic efficiency in cyclic voltammetry cycles of the $LiNi_{0.5}Mn_{1.5}O_4$ thin-film electrode.

electrochemical performance for $LiCoO_2$ thin-film electrodes [15]. Recently, Tarnopolskiy et al. reported that the charged spinel of $Li_xNi_{0.4}Mn_{1.6}O_4$ showed self-discharge with oxidative decomposition of electrolyte solutions but the self-discharge was mostly reversible [9]. The reversible behavior of the self-discharge seems to have the same origin as the good capacity retention in the CV cycles in our study. In order to detail the surface states of the $LiNi_{0.5}Mn_{1.5}O_4$ thin-film electrodes in contact with the organic electrolyte solutions, spectroscopic measurements were performed by using *ex situ* XPS and *in situ* TRF-XAS techniques.

3.3. XPS measurements

In order to analyze possible decomposition products of the organic electrolyte solutions, the surface of the $LiNi_{0.5}Mn_{1.5}O_4$ thin-film electrodes was examined by XPS. Fig. 6 compares XPS spectra of two $LiNi_{0.5}Mn_{1.5}O_4$ thin-film electrodes in the C-1s and O-1s regions. One electrode was soaked in the electrolyte solution, and it was disassembled without cycling ("after soaking"). The other electrode is disassembled after 20 CV cycles ("after 20 cycles"). Two peaks were observed in each of the C-1s and O-1s regions; a peak corresponding to C—H and C—C bonds at 284.8 eV and that corresponding to a C═O bond at 288.5eV in the C-1s region [12], and a peak for metal oxides at 529.5 eV and for C═O at 531.5 eV in the O-1s region. Increase in the peak intensity for the C═O double-bond is clear for the "after 20 cycles" electrode as compared with the "after soaking" in both the C-1s and O-1s regions. This suggests that the $LiNi_{0.5}Mn_{1.5}O_4$ thin-film electrodes become covered with a layer of carbonyl and/or carbonate compounds, probably lithium alkyl carbonates (RO(C═O)OLi), after the charge/discharge cycles [10]. The cause of the increase in the carbonyl/carbonate compounds can be the oxidative decomposition of the organic electrolyte solutions on the surface of the $LiNi_{0.5}Mn_{1.5}O_4$ thin-film electrodes.

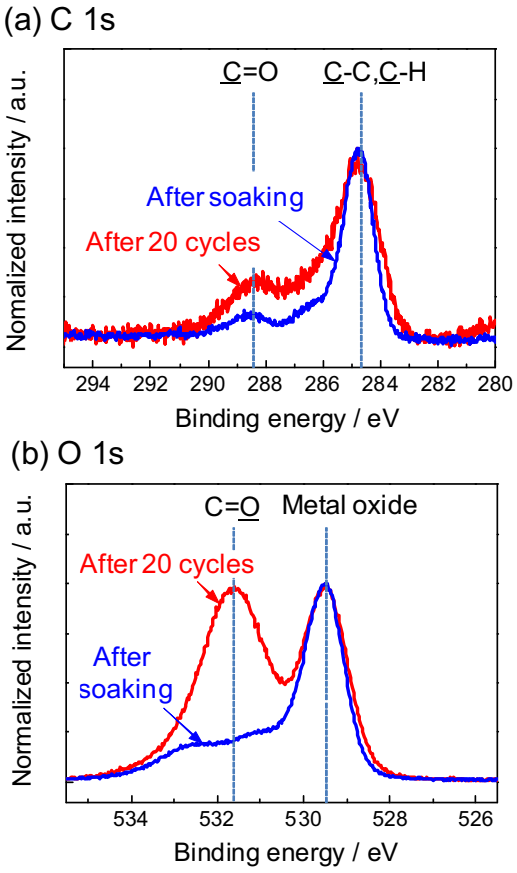

Fig. 6. XPS spectra of the $LiNi_{0.5}Mn_{1.5}O_4$ thin-film electrodes after the electrolyte soaking and after 20 CV cycles in (a) the C-1s and (b) the O-1s regions. The spectra are normalized by the intensity at 284.8 eV in the C-1s region, and that at 529.5 eV in the O-1s region.

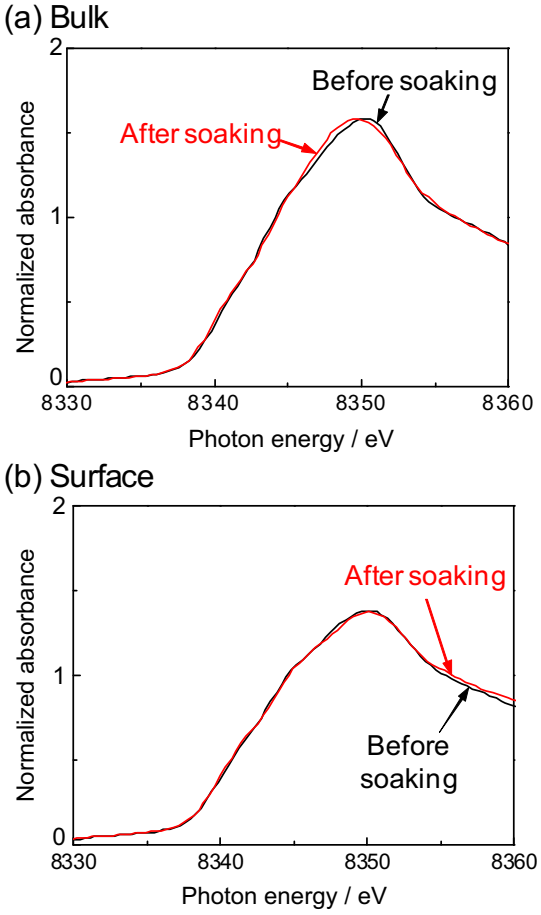

Fig. 7. Ni K-edge TRF-XAS spectra of the $LiNi_{0.5}Mn_{1.5}O_4$ thin films from (a) the bulk and (b) the surface. The black and red lines denote the spectra for the thin films before and after the electrolyte soaking, respectively. (For interpretation of the references to colour in this figure legend, the reader is referred to the web version of this article.)

3.4. *In situ* TRF-XAS measurements

As the XPS measurements were performed *ex situ*, it was difficult to observe surface states of the $LiNi_{0.5}Mn_{1.5}O_4$ thin-film electrodes under battery operating conditions. Hence, *in situ* TRF-XAS technique was applied to the $LiNi_{0.5}Mn_{1.5}O_4$ thin-film electrodes to examine their surface states during the electrochemical tests. Fig. 7 shows Ni K-edge TRF-XAS spectra of the $LiNi_{0.5}Mn_{1.5}O_4$ thin films obtained from the bulk and the surface before and after electrolyte soaking, and Fig. 8 shows the corresponding Mn K-edge TRF-XAS spectra. Before soaking the spectra from the surface are very similar to those from the bulk for both Ni and Mn K-edges, and no difference in energy at the edge or peak top can be seen between the surface and bulk. Moreover, the electrolyte soaking does not change the spectra from either the bulk or the surface for both edges. These results suggest that the chemical states and local environments of both nickel and manganese species at the surface of $LiNi_{0.5}Mn_{1.5}O_4$ are almost the same as those in the bulk, and both species are chemically stable against the organic electrolyte solution.

Fig. 9 shows Ni K-edge TRF-XAS spectra of the $LiNi_{0.5}Mn_{1.5}O_4$ thin-film electrodes from the bulk and the surface obtained under battery operating conditions of controlled potential; after soaking (ca. 2.9 V), at 4.74 V that is the middle of the two current peaks in the CV cycles shown in Fig. 4, and at 4.9 V. It is clear that the spectra from the bulk monotonically shift toward the higher-energy side as the higher potential is applied, suggesting increase in the oxidation state of the nickel species from +2 before charging ("after soaking") to +4 at 4.9 V. Furthermore, it is clearly seen that the TRF-XAS spectra at the surface exhibit energy shift toward the higher-energy side upon charging in the same manner as the spectra in the bulk. This indicates that the nickel species at the surface of the $LiNi_{0.5}Mn_{1.5}O_4$ thin-film electrodes have almost the same electrochemical activity as that in the bulk.

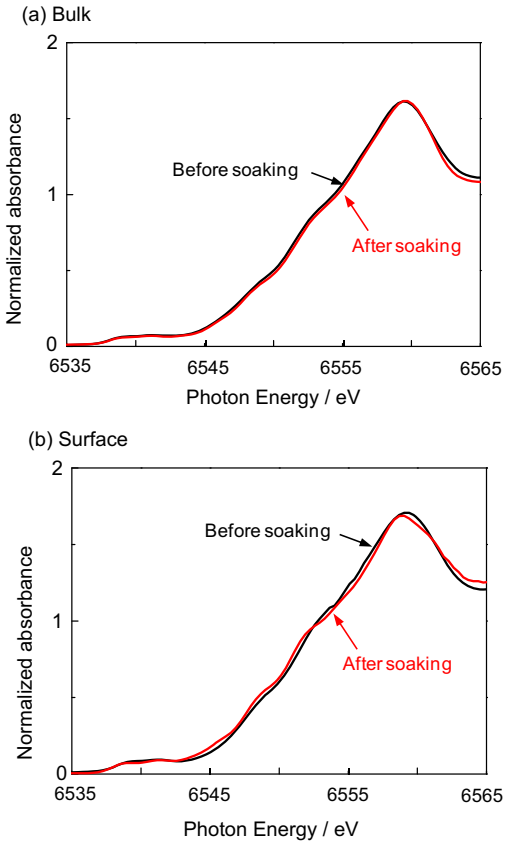

Fig. 8. Mn K-edge TRF-XAS spectra of the $LiNi_{0.5}Mn_{1.5}O_4$ thin films from (a) the bulk and (b) the surface. The black and red lines denote the spectra for the thin films before and after the electrolyte soaking, respectively. (For interpretation of the references to colour in this figure legend, the reader is referred to the web version of this article.)

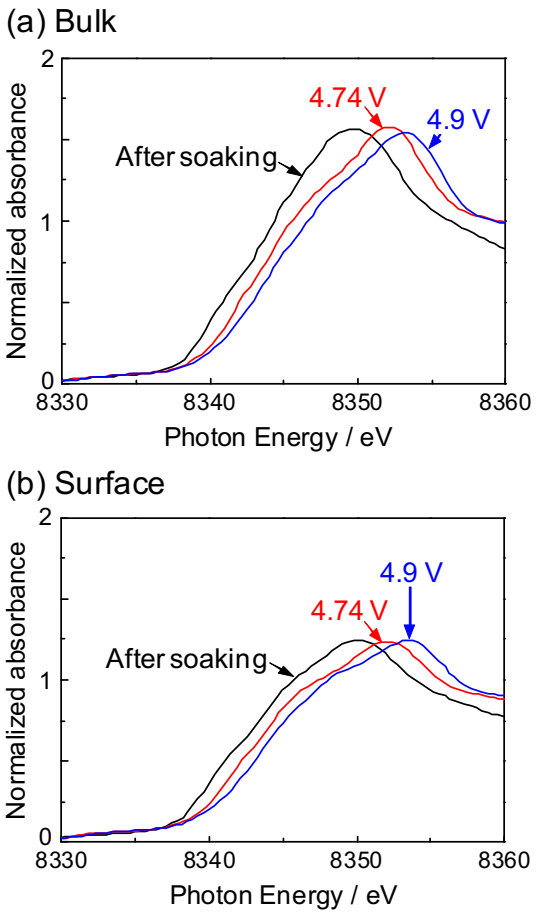

Fig. 9. Ni K-edge TRF-XAS spectra of the $LiNi_{0.5}Mn_{1.5}O_4$ thin-film electrodes after the electrolyte soaking, at 4.74 V and at 5.0 V from (a) the bulk and (b) the surface, respectively.

The TRF-XAS measurements revealed that the nickel and manganese species at the surface of the $LiNi_{0.5}Mn_{1.5}O_4$ electrodes has almost the same chemical states and local environments as those in the bulk when in contact with the organic electrolyte solutions, and that the nickel species is monotonically oxidized during the charging process in the same manner as in the bulk. The surface characteristics of $LiNi_{0.5}Mn_{1.5}O_4$ are in sharp contrast with those of $LiCoO_2$, in which the cobalt species at the surface is reduced by the contact with the organic electrolyte solutions and the surface cobalt species shows poor electrochemical behavior in the cycling [15]. In the case of $LiNi_{0.5}Mn_{1.5}O_4$, excess charging current flows (with limited coulombic efficiency per cycle) and thus the decomposition of the organic electrolyte solutions occurs at the high operating potential, as suggested by the XPS measurements. But the electrolyte decomposition does not cause the irreversible change of the surface states of $LiNi_{0.5}Mn_{1.5}O_4$. As a result, the decomposed products form a protective surface layer on the surface of the $LiNi_{0.5}Mn_{1.5}O_4$ electrodes. This resistible character of the surface against the irreversible reduction by the organic electrolyte solutions would be the nature of $LiNi_{0.5}Mn_{1.5}O_4$, and this would be the origin of its comparatively good cycling characteristics in spite of the high operating potential.

4. Conclusion

The phenomena at the electrode/electrolyte interface of $LiNi_{0.5}Mn_{1.5}O_4$ were studied using the flat and well-defined thin films as model electrodes. The TRF-XAS measurements revealed that both the nickel and manganese species at the surface of the $LiNi_{0.5}Mn_{1.5}O_4$ electrodes have almost the same chemical states and local environments as those in the bulk when in contact with the organic electrolyte solutions. The surface nickel species is monotonically oxidized during the charging process in the same manner as that in the bulk. The decomposition of the organic electrolyte solution occurs at the high operating potential, as suggested by the XPS measurements. However, the electrolyte decomposition does not lead to the irreversible change of the surface states of $LiNi_{0.5}Mn_{1.5}O_4$, which is in sharp contrast with the case of $LiCoO_2$. As a result, the decomposed products form a protective surface layer on the surface. This resistible character of the surface against the irreversible reduction by the organic electrolyte solutions would be the nature of $LiNi_{0.5}Mn_{1.5}O_4$, and this would be the origin of its comparatively good cycling characteristics in spite of the high operating potential.

Acknowledgments

This work was supported by Research and Development Initiative for Scientific Innovation of New Generation Batteries (RISING) project from New Energy and Industrial Technology Department Organization (NEDO) in Japan. The *in situ* TRF-XAS experiments in this study were carried out at the BL01B1 of SPring-8 with the approval of the Japan Synchrotron Radiation Research Institute (JASRI) (Proposal No. 2010B1027, 2011A1009, and 2011A1011) and at the BL28XU (Proposal No. 2012A7600).

References

[1] C. Sigala, D. Guyomard, A. Verbaere, Y. Piffard, M. Tournoux, Solid State Ionics 81 (1995) 167.
[2] Q. Zhong, A. Bonakdarpour, M. Zhang, Y. Gao, J.R. Dahn, J. Electrochem. Soc. 144 (1997) 205.
[3] H. Kawai, M. Nagata, H. Kageyama, H. Tukamoto, A.R. West, Electrochim. Acta 45 (1999) 315.
[4] T. Ohzuku, S. Takeda, M. Iwanaga, J. Power Sources 81–82 (1999) 90.
[5] H. Shigemura, H. Sakaebe, H. Kageyama, H. Kobayashi, A.R. West, R. Kanno, S. Morimoto, S. Nasu, M. Tabuchi, J. Electrochem. Soc. 148 (2001) A730.
[6] Y.E. Eli, W.F. Howard Jr., S.H. Lu, S. Mukerjee, J. Mcbreen, J.T. Vaughey, M.M. Thackeray, J. Electrochem. Soc. 145 (1998) 1238.
[7] J.H. Kim, S.T. Myung, Y.K. Sun, Electrochim. Acta 49 (2004) 219.
[8] H.Y. Xu, S. Xie, N. Ding, B.L. Liu, Y. Shang, C.H. Chen, Electrochim. Acta 51 (2006) 4352.
[9] V. Tarnopolskiy, J. Kalhoff, M. Nádherná, D. Bresser, L. Picard, F. Fabre, M. Rey, S. Passerini, J. Power Sources 236 (2013) 39.
[10] D. Aurbach, B. Markovsky, G. Salitra, E. Markevich, Y. Talyossef, M. Koltypin, L. Nazar, B. Ellis, D. Kovacheva, J. Power Sources 165 (2007) 491.
[11] L. Wang, H. Li, X. Huang, Prog. Nat. Sci. 22 (2012) 207.
[12] L. Yang, B. Ravdel, B.L. Luchta, Electrochem. Solid-state Lett. 13 (2010) A95.
[13] K.J. Carroll, M.-C. Yang, G.M. Veith, N.J. Dudney, Y.S. Meng, Electrochem. Solid-state Lett. 15 (2012) A72.
[14] D. Aurbach, B. Markovsky, Y. Talyossef, G. Salitra, H.-J. Kim, S. Choi, J. Power Sources 162 (2006) 780.
[15] D. Takamatsu, Y. Koyama, Y. Orikasa, S. Mori, T. Nakatsutsumi, T. Hirano, H. Tanida, H. Arai, Y. Uchimoto, Z. Ogumi, Angew. Chem. Int. Edit. 51 (2012) 11597.
[16] N. Amdouni, K. Zaghib, F. Gendron, A. Mauger, C.M. Julien, Ionics 12 (2006) 117.
[17] Y. Idemoto, H. Narai, N. Koura, J. Power Sources 119–121 (2003) 125.
[18] J.-H. Kim, C.S. Yoon, S.-T. Myung, J. Prakash, Y.-K. Sun, Electrochem. Solid-state Lett. 7 (2004) A216.
[19] J.-H. Kim, S.-T. Myung, C.S. Yoon, S.G. Kang, Y.-K. Sun, Chem. Mater. 16 (2004) 906.
[20] L. Wang, H. Li, X. Huang, E. Baudrin, Solid State Ionics 193 (2011) 32.
[21] H. Xia, Y.S. Meng, L. Lu, G. Ceder, J. Electrochem. Soc. 154 (2007) A737.